Journal of Power Sources 196 (2011) 147–152

Contents lists available at ScienceDirect

Journal of Power Sources

journal homepage: www.elsevier.com/locate/jpowsour

Improvement of proton-exchange membrane fuel cell performance using platinum-loaded carbon black entrapped in crosslinked chitosan

Waranya Phompan, Nanthiya Hansupalak*

Department of Chemical Engineering, Faculty of Engineering, Kasetsart University, 50 Paholyothin Rd., Jatujak, Bangkok 10900, Thailand

ARTICLE INFO

Article history:
Received 10 April 2010
Received in revised form 20 June 2010
Accepted 28 June 2010
Available online 13 July 2010

Keywords:
Proton-exchange membrane fuel cell
Carbon black support
Chitosan
Crosslink
Platinum catalyst

ABSTRACT

To improve the performance of proton-exchange membrane fuel cells which use hydrogen and oxygen as fuels, the application of small proton-conducting polymer to extend the three-phase boundary into the primary pores of catalyst-loaded carbon black agglomerates is of interest. An alternative and simple crosslinking method is proposed in place of the complicated polymer-grafting methods. Platinum-loaded carbon black is entrapped in epichlorohydrin-crosslinked chitosan of low molecular weight. Morphology and pore analyses of carbon black prior and post treatment are assessed, as well as performances of fuel cells fabricated with the treated and the untreated carbon black at 40 °C and 100% humidity. Results indicate the existence of chitosan chains in the primary pores of the carbon black agglomerates, corresponding to a decline in the activation overvoltage and resulting in significantly better cell performance. An increase in chitosan amount, however, does not necessarily enhance the cell performance because effects of ohmic and concentration losses may become more dominant than that of the raised exchange current density of the cell.

1. Introduction

A H_2/O_2 proton-exchange membrane fuel cell (PEMFC) is considered a clean, sustainable energy source and suitable for the operation of small electronic devices [1]. Such fuel cells were invented in 1960s, but the high cost of precious platinum, used as a catalyst for H_2 oxidation and O_2 reduction, has hindered the commercialization of PEMFCs. This is, however, no longer the case as many techniques which reduce the platinum loading from 28 to 0.4 mg cm^{-2} or less without lowering fuel cell performance have been reported on since 1993 [2–5]. In fact, numerous problems delaying the commercialization of PEMFCs lie in the electrode layers, such as sluggish reaction kinetics and poor mass transport of protons and electrons [6].

Activation overvoltage, or activation loss, of a fuel cell resulting from slow reactions in electrodes appreciably influences the voltage drop at low-temperature operation, but becomes insignificant at high temperature and high pressure [5]. To lessen the activation overvoltage for low-temperature operation, a three-phase boundary, comprising ionomer, catalyst and gas phases, needs to be formed to push the redox reactions forward in electrodes [5,7]. In this regard, a proton-conducting polymer (e.g., Nafion™ and Flemion®) is incorporated in the electrode layers, which are typically made of a carbon black-supported catalyst. A problem associated with the use of carbon black, which cannot be dispensed with, is the tendency of carbon black to be agglomerated due to its fine size and van der Waals force. The interspaces between carbon black particles in an agglomerate, alternatively called primary pores, are less than 40 nm in diameter, while those between agglomerates, known as secondary pores, are within the diameter range of 40–1000 nm [8,9]. As a result, ionomer molecules with molecular weights of the order of several hundred thousand grams per mole cannot penetrate the primary pores and only remain in the secondary pores [8,10,11]. It has been reported [12,13] that catalyst particles which are inaccessible to large ionomer chains cannot participate in the redox reactions owing to the lack of the three-phase boundary, which leads to the raised activation overvoltage and, consequently, decreased cell performance.

Following the aforementioned findings, catalyst accessibility can be enhanced by a variety of methods that can be classified into two main categories: (i) extension of the three-phase boundary areas into the primary pores of catalyst-loaded carbon black and (ii) restriction of the three-phase boundary areas to the secondary pores only. The concept of the first category is associated with the utilization of negatively charged monomers in conjunction with graft polymerization to ensure better pore penetration and the stability of contacts between the ionomer chains and the carbon black particles [14]. Additionally, to improve mass transport of reactant gases inside the primary pores, the long polyelectrolyte chains grafted on the carbon surfaces are replaced by small

* Corresponding author. Tel.: +66 2579 2083; fax: +66 2561 4621.
E-mail address: fengnyh@ku.ac.th (N. Hansupalak).

0378-7753/$ – see front matter © 2010 Elsevier B.V. All rights reserved.
doi:10.1016/j.jpowsour.2010.06.110

Table 1
List of ingredients to prepare chitosan-entrapped Pt/C.

Catalyst	Chitosan solution (mL)	Epichlorohydrin (mL)	Crosslinking time (h)	Chitosan content in catalyst (wt.%)
Pt/C	0	0	0	0
Chi-4-Pt/C	5	1	1	4
Chi-10-Pt/C	15	1	1	10

proton-conducting molecules (e.g., sodium sulfite) [15]. The second category is based on a concept that, prior to the catalyst impregnation, the primary pores of bare carbon black are blocked by ionomer molecules that are either ready-made and large enough to reside in the secondary pores only [16,17], or formed by polymerization of monomers present in the primary pores [18]. Thus, by blocking the primary pores of the carbon black with large ionomer, only secondary pores are impregnated with metal catalyst.

As the surface of carbon black is inert to any grafting, the techniques mentioned above must rely on functionalization of the surface to generate active sites that can anchor molecules. For graft polymerization, some initiator molecules may bind to the carbon black surface via a one-step or a multi-step functionalization. As an example of the former case, the carbon black surface is functionalized with alcoholic hydroxyl groups, which are used along with ceric ions to initiate free-radical polymerization [14]. The example of the latter is functionalization of the carbon black surface with carboxyl groups followed by their conversion to acyl chloride groups, which can form chemical bonds with azo-initiator molecules to attain free-radical polymerization. [18]. It should be noted that, during a grafting process, direct contact between catalyst-loaded carbon black and organic solvent may cause spontaneous combustion [14], which calls for cautious handling.

To summarize, the techniques described above can be deemed complex and may prolong the procedures to obtain the desired carbon products in excess of 24 h. To avoid the complications of catalyst impregnation and grafting techniques, a simple and swift method (i.e., the utilization of small ionomer chains, which can access the primary pores, in entrapment of catalyst-loaded carbon black) is proposed. Covalent crosslinking of the ionomer chains is exploited to ensure the adherence of such small polymer chains to carbon black particles. To reach the goal, low molecular-weight chitosan was chosen to represent the ionomer mentioned above because of its high glass transition temperature in addition to its two different functional groups: –OH and $–NH_2$. Only the former functional group can be covalently crosslinked with epichlorohydrin to form the network structure [19], while the latter group is free to attract proton and water molecules (both of which contribute to the proton mitigation). Furthermore, this method is not only simple and rapid, but also safe as it allows the catalyst-loaded carbon black to be in contact with water and, consequently, reduces the risk of fire.

This work aims to demonstrate that platinum-loaded carbon black entrapped in crosslinked chitosan can enhance H_2/O_2 fuel cell performance. The performance of fuel cells assembled with the treated carbon black at 40 °C and 100% humidity is scrutinized and compared with fuel cells fabricated with untreated carbon black under the same test conditions. Furthermore, to analyze the effectiveness of the method on cell performance, the morphology and N_2 sorption isotherms of carbon black entrapped in a chitosan network of varied chitosan content are examined.

2. Experimental

2.1. Materials

Platinum, HiSPEC 4000, nominally 40% on carbon black (#42204, named Pt/C) was purchased from Alfa Aesar. Chitosan (Mn ~ 20k, 87% deacetylation, PDI ~ 6) was obtained from A.N. Lab, Thailand; whereas acetic acid, epichlorohydrin, and sodium hydroxide were acquired from Sigma–Aldrich, Acros Organic, and MERCK, respectively. Prior to use, the Pt/C was dried overnight in a vacuum oven at 80 °C. All other chemicals were used without any prior treatment.

2.2. Entrapment of Pt/C in covalently crosslinked chitosan

A 1 wt.% chitosan solution in 1 wt.% acetic acid was added to a round-bottom flask that contained 1 g of oven-dried Pt/C. The solution was subjected to pulsed ultrasonication by means of a Cole-Parmer 500 W ultrasonic processor (model CP505, 25% amplitude) for a period of 10 min. The dispersion was then well mixed with epichlorohydrin via the same ultrasonic treatment and subsequent stirring, prior to the application of heat under reflux at 50 °C for 1 h. Next, a 0.1 M NaOH solution was added and the resulting mixture was boiled for a period of time, which was denoted as the crosslinking time. Afterwards, the mixture was washed and decanted using the following solutions in sequence: deionized water, 0.1 M HCl, 0.1 M NaOH, and deionized water. It was subsequently dried overnight at 80 °C under vacuum until a constant weight was attained. The amounts of some of the aforementioned ingredients for the preparation of the Pt/C entrapment are summarized in Table 1.

2.3. Fabrication of MEA and measurement of cell performance

The ink solution for the control run consisted of isopropanol, deionized water, a commercial Liquion™ 1100 Nafion solution (Ion Power, Inc.), and Pt/C in an amount that yielded a platinum loading of 0.4 mg cm^{-2}. The same recipe was also utilized to prepare an ink solution, in which untreated Pt/C was replaced by the same weight of the treated one. Consequently, the platinum content in the latter ink was slightly less than that in the former due to the presence of chitosan. An electrode layer with an active area of 5 cm^2 was formed on each side of a Nafion 115 membrane, all of which was subsequently assembled with gas-diffusion layers by the hot pressing method [20].

Fuel cell performance was evaluated with an in-house fuel cell test station under atmospheric pressure [20]. Hydrogen and oxygen gases were fed to the anode and cathode sides at flow rates of 0.2 and 0.1 mL min^{-1}, respectively. The humidifier and cell temperatures were identical and kept constant at 40 °C.

2.4. BET analysis and morphology

Nitrogen sorption isotherms and pore-size distributions for both non- and chitosan-entrapped Pt/C were determined at 77 K using an Autosorb-1 surface area analyzer (Quantachrome, Science Engineering). The samples were dried at 100 °C for 8 h prior to the measurement. The morphology of treated and untreated Pt/C was characterized by a JEOL JSM-6301F scanning electron microscope (SEM) and a JEOL JEM-2010 transmission electron microscope (TEM).

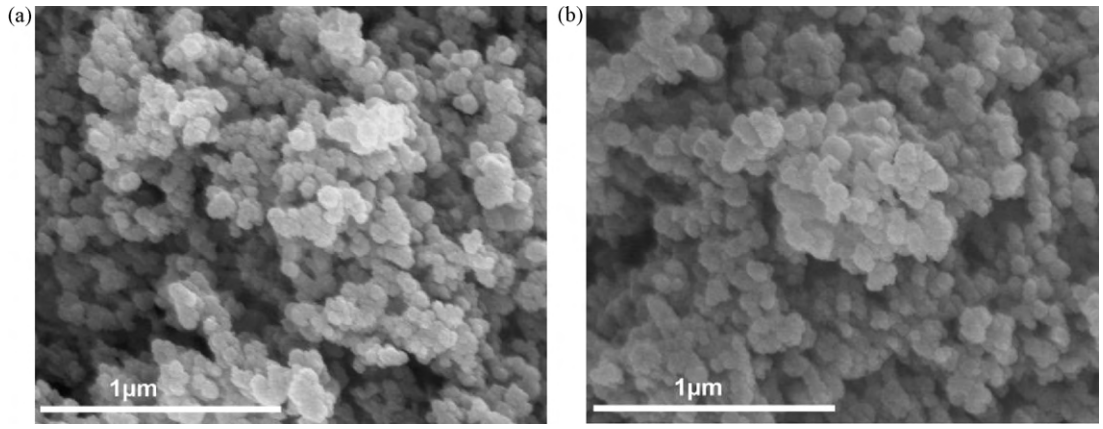

Fig. 1. SEM images of catalysts: (a) Pt/C and (b) Chi-4-Pt/C (Magnification: 50 000×).

3. Results and discussion

3.1. Morphology of treated and untreated Pt/C

The scanning electron micrograph in Fig. 1a displays the tendency of naturally occurring agglomeration of Pt/C, which is enhanced by the entrapment of Pt/C in chitosan (Fig. 1b). In addition, the comparable sizes and similar shapes of individual particles in the agglomerates of Pt/C and Chi-4-Pt/C are easily observable with the aid of TEM, as shown in Fig. 2a and b, respectively. These observations indicate that chitosan thinly covers the Pt/C particles, and thereby results in the occurrence of a greater content of agglomerates.

3.2. N_2 sorption isotherms and pore-size distributions

It should be noted that, in addition to micropores and mesopores, the N_2 sorption technique can be used to characterize macropores with pore diameters in the range of 40–100 nm. The technique yields results that are comparable with those measured

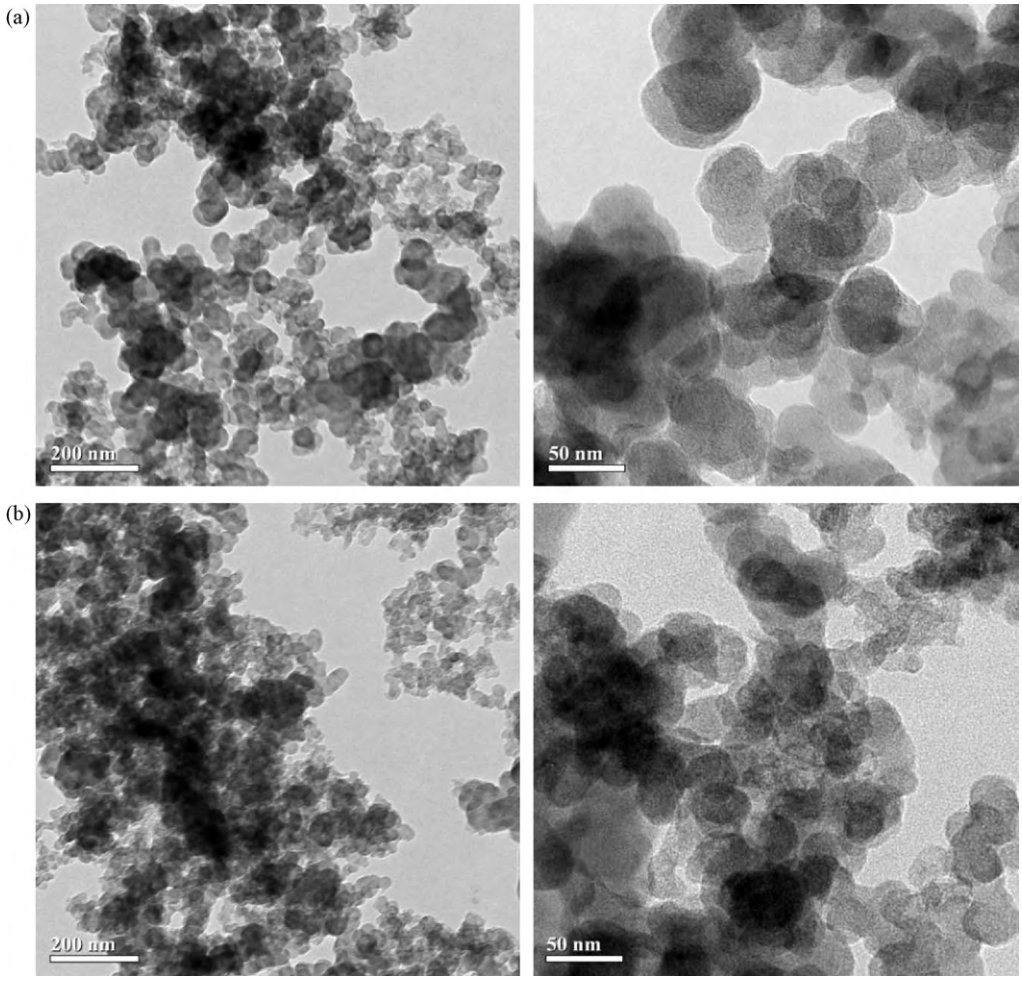

Fig. 2. TEM images of catalysts: (a) Pt/C and (b) Chi-4-Pt/C. Magnifications of left and right images are 20 000 and 60 000, respectively.

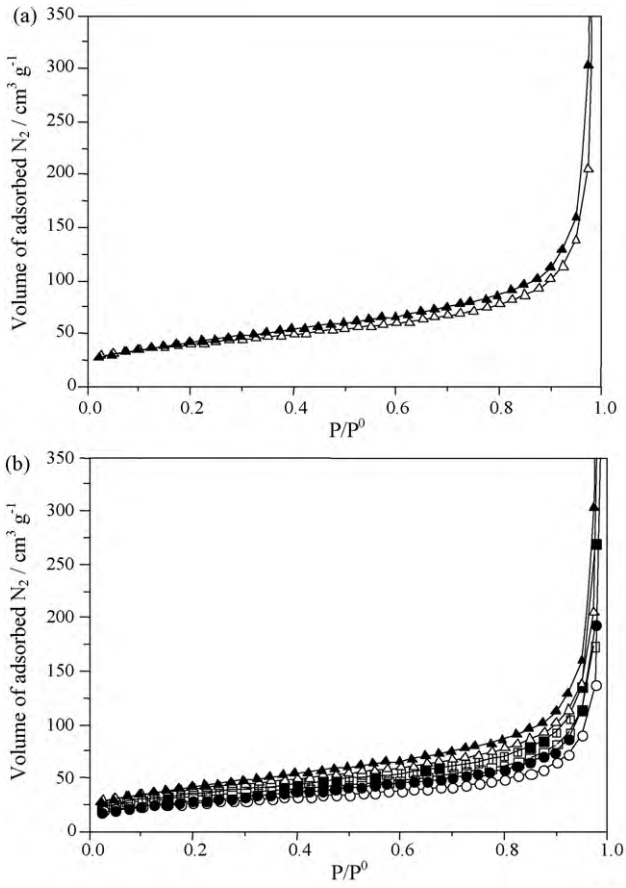

Fig. 3. N_2 sorption isotherms of (a) Pt/C (triangles) and (b) Pt/C (triangles) in comparison with Pt/C entrapped in varied content of chitosan at 77 K: Chi-4-Pt/C (squares) and Chi-10-Pt/C (circles). Open and closed symbols represent adsorption and desorption isotherms, respectively.

Table 2
BET specific surface area and pore volume of Pt/C with varied chitosan content.

Catalyst	BET specific surface area ($m^2\ g^{-1}$)	Pore volume ($cm^3\ g^{-1}$)
Pt/C	138	1.16
Chi-4-Pt/C	113	1.11
Chi-10-Pt/C	66	0.97

by mercury porosimetry, which is typically used to characterize macroporous materials [21,22].

The shape of the N_2 adsorption isotherm for Pt/C in Fig. 3a is identical to that of the isotherms for Chi-4-Pt/C and Chi-10-Pt/C. The isotherm is a type II in accordance with the IUPAC classification [23] and is indicative of nonporous and macroporous adsorbents. The narrow hysteresis loop (type H3) appearing in the adsorption–desorption isotherms specifies adsorbents with slit-shaped pores, formed by layers of globule agglomerates [24]. A pronounced increase in adsorption at high relative pressure implies the existence of mesopores and macropores (referred to as primary and secondary pores of the carbon black agglomerates, respectively). All of these observations reflect the characteristics of macroporous materials arising from the agglomeration of the carbon black particles (already confirmed by SEM and TEM images in Figs. 1 and 2).

In Fig. 3b, for the entire range of the relative pressure, both adsorption and desorption isotherms of chitosan-entrapped Pt/C lie beneath those of the untreated Pt/C, and thereby indicate a decline in the capacity of gas adsorption. Additionally, it is evident in Table 2

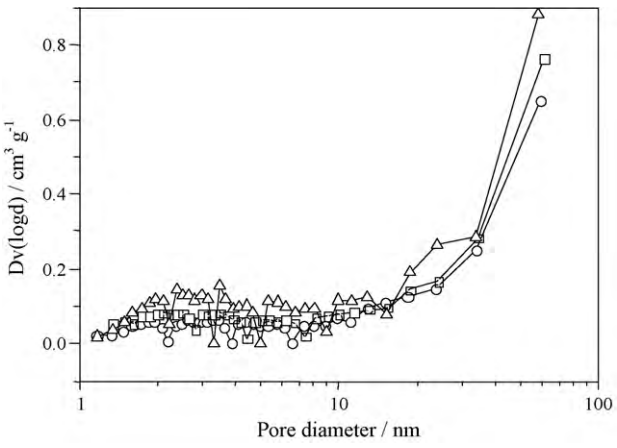

Fig. 4. Pore-size distributions of catalysts with various levels of chitosan content: Pt/C (triangles), Chi-4-Pt/C (squares), and Chi-10-Pt/C (circles).

that the reduction of the corresponding BET specific surface area and pore volume is caused by the chitosan content. Furthermore, the pore-size distributions in Fig. 4 shows a decrease in the specific volumes of pores with diameters in the range 2–60 nm on the addition of chitosan. This observation confirms the existence of chitosan in the primary and secondary pores of the carbon black agglomerates.

With an increased chitosan amount, the diminution in the specific volumes of pores of less than 40 nm diameter is, however, insignificant (see Fig. 4). This implies a higher amount of chitosan in the secondary pores for Chi-10-Pt/C, whereas chitosan is mostly present in the primary pores for Chi-4-Pt/C.

3.3. Single fuel cell tests

Polarization and power density curves displayed in Fig. 5a and b were obtained from performance tests of a single fuel cell assembled with three different catalysts (Pt/C, Chi-4-Pt/C, and Chi-10-Pt/C), while all other cell components and test conditions were kept identical. In addition, each catalyst was used to prepare both the anode and the cathode. The Marquardt method was employed to fit Eq. (1) to the polarization data in order to yield the exchange current density (i_0) and Tafel slope (b) for both electrodes, as listed in Table 3. Note that all obtained fitting R^2 values are greater than 0.99 and thereby confirm good fits.

$$V_{cell} = V_{reverse} - \eta_{act} - \eta_{ohm} - \eta_{conc} \quad (1)$$

where V_{cell} and $V_{reverse}$ are the cell and reversible voltages, respectively; η_{act}, η_{ohm}, and η_{conc} are the activation, ohmic and concentration overvoltages of the cell, respectively. The calculated overvoltages are associated with voltage losses at both electrodes [7,25]. As shown in Fig. 5a, η_{conc} is negligible and can be neglected, whereas η_{act} and η_{ohm} are derived as follows:

$$\eta_{act} = b\ \ln\left(\frac{i}{i_0}\right) \quad (2)$$

$$\eta_{ohm} = iR_{ohm} \quad (3)$$

where i and R_{ohm} are the cell current density and ohmic resistance, respectively. The latter was obtained by means of linear regression of the polarization data in the medium range of current density range, which renders fitting R^2 values higher than 0.99.

At 0.6 V the cell fabricated with Chi-4-Pt/C yields a higher current density than the cell with Pt/C, which gives the order Chi-4-Pt/C > Pt/C > Chi-10-Pt/C, as shown in Fig. 5a. The descending order of the current density values is also identical with those of the corresponding power density values at 0.6 V and maximum power

Table 3
Calculated kinetic parameters for H_2/O_2 fuel cells assembled with different catalysts.

Catalyst	Nonlinear regression fitting			Linear regression fitting	
	i_0 ($\times 10^{-7}$ A cm^{-2})	b (mV dec^{-1})	Fitting R^2	R_{ohm} (Ω cm^2)	Fitting R^2
Pt/C	7.00	20	0.995	0.51	0.997
Chi-4-Pt/C	8.24	15	0.996	0.54	0.997
Chi-10-Pt/C	9.97	29	0.996	0.65	0.996

density values, as indicated in Fig. 5b. Thus, the results clearly demonstrate superior cell performance in the presence of a small amount of chitosan in the electrode layers.

In comparing the cell performances of Pt/C and Chi-4-Pt/C in the ranges of medium and high current density (Fig. 5a), it is obvious that Chi-4-Pt/C does not significantly affect ohmic resistance and mass transport. In the lower current density region, however, the i_0 value listed in Table 3 for the cell fabricated with Chi-4-Pt/C is almost 20% higher than that for the cell made with Pt/C, while the b value is 25% decreased, which indicates a reduction in the activation overvoltage. This results in a performance improvement for the fuel cell assembled with Chi-4-Pt/C.

The amplification of i_0 of the cell due to the chitosan content signifies higher redox reaction rates, which indicates the success of the application of chitosan to extend the three-phase boundary into primary pores. It is also worth noting that the total catalyst weight was constant and identical in all experiments. Consequently, the entrapment of Pt/C in chitosan raises not only the cell performance, but also platinum utilization.

The i_0 values in Table 3 can represent the exchange current density for the oxygen reduction reaction (ORR) at the cathode because the reaction is considerably slower than the hydrogen oxidation reaction (HOR) at the anode [26]. Mizuhata et al. [14] reported i_0 values at the cathodes of H_2/O_2 fuel cells fabricated with non-grafted or polymer-grafted carbon black to be 1.5×10^{-6} and 9.5×10^{-6} A cm^{-2}, respectively, which are about one order of magnitude higher than the values in Table 3. This is mainly attributed to the higher operating temperature (60 °C) as opposed to 40 °C employed in the present work [27]. Mizuhata et al. [14] ascribed an increase in i_0 at the cathode to the presence of the polymer in the primary pores of carbon black agglomerates. Note that the Tafel slope values obtained in that study [14] are of the same order of magnitude as those reported in Table 3, albeit slightly higher due to the greater temperature effect [27]. Also, it should be added that experimental confirmation may be needed to differentiate the influence of a polymer on i_0 at the anode and the cathode.

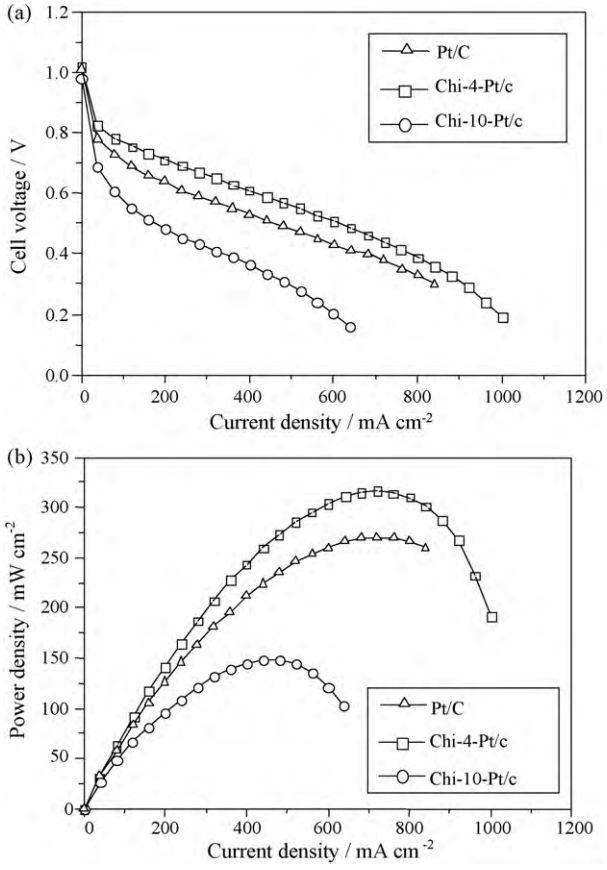

Fig. 5. (a) Polarization and (b) power density curves of fuel cells fabricated with different amounts of chitosan.

The contribution of chitosan in the primary pores to the reduction in activation overvoltage is likely to be caused by two cooperative factors: (i) the existence of good interfacial contacts between chitosan molecules and Pt/C particles; (ii) the ability of chitosan to protonate. The first factor is due to the entrapment of Pt/C particles in the network formed by chitosan molecules, which are small enough to penetrate into the primary pores of carbon black agglomerates, as depicted in Fig. 6a. The second factor is illustrated in Fig. 6b. Epichlorohydrin can form bonds with hydroxyl functional groups of chitosan and leaves the amine groups free for ionization, or protonation. In addition to ionization by protons generated at the anode, chitosan can also be protonated in water. The pK_a of chitosan, which reflects the degree of protonation, is actually 6.1–6.7 [28]; therefore, almost 50% of the amine groups per one chain is protonated in deionized water, which has a pH of approximately 6.5. Thus, there are plenty of protonated amine groups that enable proton transfer on the catalyst surface by means of the *Grotthuss mechanism*, i.e., the progression of a proton from one hydrogen bonding site of chitosan to another. Furthermore, due to its natural hydrophilic characteristics, chitosan can hold water generated in the fuel cell, which enhances proton migration via the *Vehicle mechanism*.

Although a small amount of chitosan boosts fuel cell performance, the cell fabricated with Chi-10-Pt/C (Fig. 5a and b) possesses the poorest performance. Chi-10-Pt/C, which contains greater amounts of chitosan than Chi-4-Pt/C, yields higher values for i_0, b, and R_{ohm}, as indicated Table 3. The larger values for b and R_{ohm} imply higher activation and ohmic overvoltages, which both hinder the effect of an increased i_0 on the cell performance. Furthermore, the mass transport problem in the cell fabricated with Chi-10-Pt/C is detected at a much lower current density. These signs of poor performance can be attributed to the excessive amount of chitosan present in the pores of Pt/C, which causes: (i) an alteration of the state of the reactive surface; (ii) the obstruction of gas transport to reactive sites; (iii) resistance to electron flow and contact resistance.

The likely cause of the higher R_{ohm} values for the cell fabricated with Chi-10-Pt/C is twofold. First, the absence of strong bonds between the polymer and carbon black particles, which can inhibit polymer movement, as well as the dissimilar thermal expansion coefficients of polymer and carbon black particles is responsible for the increase in the electrical resistivity of polymer–carbon black composites [29] that, in the present work, appears to be correlated to the amount of chitosan. Second, the difference in volume change

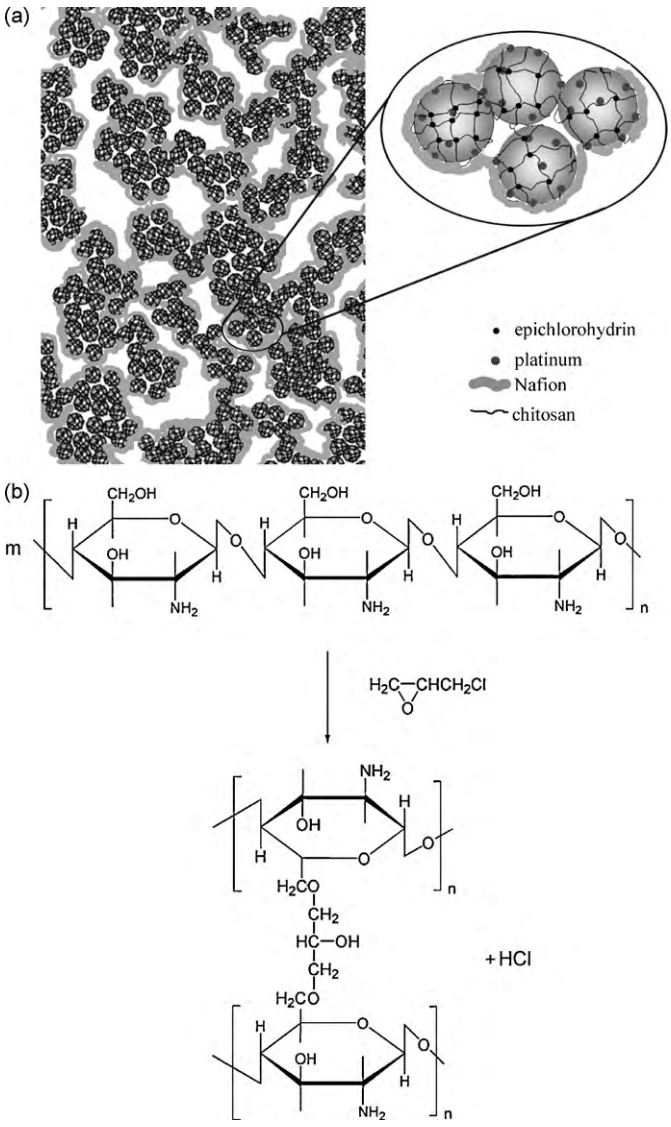

Fig. 6. (a) Scheme of platinum-loaded carbon black entrapped in crosslinked low molecular-weight chitosan. Nafion chains only remain in the secondary pores of the carbon black due to its high molecular weight. (b) Crosslinking of chitosan molecules with use of epichlorohydrin molecules.

of Nafion and other hydrocarbon polyelectrolytes under identical thermal and aqueous conditions and identical fuel cell operating conditions causes local interfacial delamination, which consecutively triggers an increase in the contact resistance [30–32]. The current work, as evident in Fig. 4, reveals the possibility of increased levels of chitosan in the secondary pores for Chi-10-Pt/C, compared with Chi-4-Pt/C, and this is responsible for the boosted numbers of chitosan–Nafion contacts. This indicates the cause of the inferior performance of the cell assembled with Chi-10-Pt/C.

4. Conclusions

Performance improvement of a fuel cell using H_2 and O_2 by the utilization of a small proton-conducting polymer to extend the three-phase boundary into the primary pores of platinum-loaded carbon black agglomerates can be successfully achieved by the application of a straightforward method that is related to the entrapment of the carbon black particles in epichlorohydrin-crosslinked chitosan. The superior performance of the fuel cell assembled with treated carbon black is due to the reduction of the activation overvoltage, that stems from the higher exchange current density and lower Tafel slope. This is associated with the presence of chitosan in the primary pores of carbon black agglomerates, as is experimentally confirmed by BET analysis. Despite an elevated exchange current density with an increased amount of chitosan in the electrode layers, augmented levels of chitosan do not necessarily cause an improvement in the cell performance. This is because excessive chitosan greatly enlarges the Tafel slope and the correlated activation overvoltage, as well as both ohmic and concentration losses. Nevertheless, chitosan can be of use as a promising ionomer for accelerating redox reaction rates in electrodes.

Acknowledgements

We gratefully acknowledge financial support from Center of Excellence for Petroleum, Petrochemicals and Advanced Materials, S&T Postgraduate Education and Research Development Office (PERDO), and Kasetsart University Research and Development Institute (KURDI). Although results are not shown here, this work could not be done without a generous gift from the Cabot Corporation (Thailand and USA), whose Vulcan® XC72 was utilized for testing the method prior to its application to platinum-loaded carbon black of similar particle size. Finally, we thank Prof. T. Vatanatham and Prof. S. Limtrakul, Kasetsart University, Thailand for helpful discussions.

References

[1] S. Srinivasan, Fuel Cells: From Fundamentals to Applications, Springer, USA, 2006.
[2] G.S. Kumar, M. Raja, S. Parthasarathy, Electrochim. Acta 40 (1995) 285–290.
[3] M.S. Wilson, Membrane catalyst layer for fuel cells, US Patent 5,234,777 (1993).
[4] R. O'Hayre, S.J. Lee, S.W. Cha, F.B. Prinz, J. Power Sources 109 (2002) 483–493.
[5] J. Larminie, A. Dicks, Fuel Cell Systems Explained, John Wiley & Sons, England, 2003.
[6] S. Litster, G. McLean, J. Power Sources 130 (2004) 61–76.
[7] R. O'Hayre, Micro scale electrochemistry: application to fuel cells, Ph.D. Thesis, Department of Materials Science and Engineering, Stanford University, USA, 2004.
[8] M. Uchida, Y. Fukuoka, Y. Sugawara, N. Eda, A. Ohta, J. Electrochem. Soc. 143 (1996) 2245–2252.
[9] M. Watanabe, M. Tomikawa, S. Motoo, J. Electroanal. Chem. 195 (1985) 81–93.
[10] M. Uchida, Y. Aoyama, N. Eda, A. Ohta, J. Electrochem. Soc. 142 (1995) 4143–4149.
[11] N. Limjeerajarus, Y. Nishiyama, H. Ohashi, T. Ito, T. Yamaguchi, J. Chem. Eng. Jpn. 42 (2009) 616–631.
[12] M. Uchida, Y. Aoyama, N. Eda, A. Ohta, J. Electrochem. Soc. 142 (1995) 463–468.
[13] J. McBreen, J. Electrochem. Soc. 132 (1985) 1112–1116.
[14] H. Mizuhata, S.i. Nakao, T. Yamaguchi, J. Power Sources 138 (2004) 25–30.
[15] H. Kuroki, T. Yamaguchi, J. Electrochem. Soc. 153 (2006) A1417–A1423.
[16] E.J. Taylor, E.B. Anderson, N.R.K. Vilambi, J. Electrochem. Soc. 139 (1992) L45–L46.
[17] M.S. Löffler, B. Groß, H. Natter, R. Hempelmann, T. Krajewski, J. Divisek, Phys. Chem. Chem. Phys. 3 (2001) 333–336.
[18] M. Carmo, T. Roepke, C. Roth, A.M.d. Santos, J.G.R. Poco, M. Linardi, J. Power Sources 191 (2009) 330–337.
[19] F. Xi, J. Wu, React. Funct. Polym. 66 (2006) 682–688.
[20] H. Leelasupakorn, The activation losses in a proton exchange membrane fuel cell, M.E. Thesis, Department of Chemical Engineering, Kasetsart University, Thailand, 2008.
[21] S. Kang, J.S. Yu, M. Kruk, M. Jaroniec, Chem. Commun. (2002) 1670–1671.
[22] B. Holland, J. Porous Mater. 10 (2003) 17–22.
[23] K.S.W. Sing, D.H. Everett, R.A.W. Haul, L. Moscou, R.A. Pierotti, J. Rouquerol, T. Siemienewska, Pure Appl. Chem. 57 (1985) 603–619.
[24] S.H. Gregg, K.S. Sing, Adsorption, Surface Area and Porosity, Academic Press, USA, 1967.
[25] B. Gou, W.K. Na, B. Diong, Fuel Cells: Modeling, Control, and Applications, in: Power Electronics and Applications Series, CRC Press, USA, 2009.
[26] R. O'Hayre, S.W. Cha, W. Colella, F.B. Prinz, Fuel Cell Fundamentals, John Wiley & Sons, USA, 2006.
[27] A.J.J. Kadjo, P. Brault, A. Caillard, C. Coutanceau, J.P. Garnier, S. Martemianov, J. Power Sources 172 (2007) 613–622.
[28] J.W. Park, K.H. Choi, Bull. Korean Chem. Soc. 4 (1983) 68–72.
[29] S.J. Park, H.C. Kim, H.Y. Kim, J. Colloid Interface Sci. 255 (2002) 145–149.
[30] B. Yang, A. Manthiram, Electrochem. Commun. 6 (2004) 231–236.
[31] S. Song, G. Wang, W. Zhou, X. Zhao, G. Sun, Q. Xin, S. Kontou, P. Tsiakaras, J. Power Sources 140 (2005) 103–110.
[32] H.Y. Jung, J.K. Park, Int. J. Hydrogen Energy 34 (2009) 3915–3921.